Mon. Not. R. Astron. Soc. **376,** 919–928 (2007) doi:10.1111/j.1365-2966.2007.11564.x

The mass and radius of the M-dwarf in the short-period eclipsing binary RR Caeli

P. F. L. Maxted,[1,2]★ D. O'Donoghue,[3] L. Morales-Rueda,[4,2] R. Napiwotzki[5] and B. Smalley[1]

[1]*Astrophysics Group, Keele University, Staffordshire ST5 5BG*
[2]*University of Southampton, Department of Physics & Astronomy, Highfield, Southampton S017 1BJ*
[3]*South African Astronomcal Observatory, PO Box 9, Observatory 7935, Cape Town, South Africa*
[4]*Department of Astrophysics, University of Nijmegen, PO Box 9010, 6500 GL Nijmegen, The Netherlands*
[5]*Centre for Astrophysics Research, STRI, University of Hertfordshire, Hatfield AL10 9AB*

Accepted 2007 January 29. Received 2006 December 1; in original form 2006 September 6

ABSTRACT

We present new photometry and spectroscopy of the eclipsing white dwarf–M-dwarf binary star RR Cae. We use timings of the primary eclipse from white-light photo-electric photometry to derive a new ephemeris for the eclipses. We find no evidence for any period change greater than $|\dot{P}|/P \approx 5\times10^{-12}$ over a time-scale of 10 yr. We have measured the effective temperature of the white dwarf, $T_{\rm WD}$, from an analysis of two high resolution spectra of RR Cae and find $T_{\rm WD} = 7540\,{\rm K} \pm 175\,{\rm K}$. We estimate a spectral type of M4 for the companion from the same spectra. We have measured the radial velocity of the white dwarf from the Balmer absorption lines and find that the semi-amplitude of the spectroscopic orbit is $K_{\rm WD} = 79.3 \pm 3.0\,{\rm km\,s^{-1}}$. We have combined our radial velocity measurements of the M-dwarf with published radial velocities to determine a new spectroscopic orbit for the M-dwarf with a semi-amplitude of $K_{\rm M} = 190.2 \pm 3.5\,{\rm km\,s^{-1}}$. We have combined this information with an analysis of the primary eclipse to derive relations between the inclination of the binary and the radii of the two stars. We use cooling models for helium white dwarfs with a wide range of hydrogen layer masses to determine the likely range of the white dwarf radius and, thus, the inclination of the binary and the mass and radius of the M-dwarf. The mass of the M-dwarf is (0.182–0.183) $\pm$ 0.013 $M_\odot$ and the radius is (0.203–0.215) $\pm$ 0.013 $R_\odot$, where the ranges quoted for these values reflect the range of white dwarf models used. In contrast to previous studies, which lacked a measurement of $K_{\rm WD}$, we find that the mass and radius of the M-dwarf are normal for an M4 dwarf. The mass of the white dwarf is $0.440 \pm 0.022\,M_\odot$. With these revised masses and radii we find that RR Cae will become a cataclysmic variable star when the orbital period is reduced from its current value of 7.3 h to 121 min by magnetic braking in 9–20 Gyr. We note that there is night-to-night variability of a few seconds in the timing of primary eclipse caused by changes to the shape of the primary eclipse. We speculate as to the possible causes of this phenomenon.

Key words: binaries: eclipsing – stars: individual: RR Cae – white dwarfs.

1 INTRODUCTION

RR Cae is a cool white dwarf star which is eclipsed by an M-dwarf companion every 7.3 h. The eclipses were first reported by Krzeminski (1984) in a short report which also mentions that the 'radial-velocity amplitude (of the dMe star) throughout the orbit is 370 km s^{-1}'. An *R*-band light curve has been presented by Bruch & Diaz (1998) together with a single spectrum covering the wavelength region 5806–7116 Å from which they derive a spectral type for the M-dwarf companion of M5V or M6V. A more complete history of the study of this star can be found therein. Bruch (1999) presented further spectroscopy around the Hα line from which he derives a spectroscopic orbit for the M-dwarf. This information was combined with an analysis of the *R*-band light curve to estimate the masses and radii of the stars. Both Bruch & Diaz and Bruch estimated a mass of

★E-mail: pflm@astro.keele.ac.uk

about 0.09 $M_\odot$ for the M-dwarf, which is much lower than expected given its spectral type. Zuckerman et al. (2003) present a single spectrum of RR Cae taken with the HIRES echelle spectrograph on the Keck telescope. This spectrum shows several narrow absorption features at wavelengths around 390 nm due to neutral metals, for example, Al I, Fe I and Mg I, which are thought to have been accreted on to the surface of the white dwarf from the M-dwarf.

RR Cae is a double-lined eclipsing binary so it is a candidate for an accurate determination of the masses and radii of both stars. Only a few double-lined eclipsing binaries containing white dwarf stars have been identified. V471 Tau in the Hyades is perhaps the best known and longest studied such binary. The K-dwarf companion dominates the optical light of the binary so O'Brien, Bond & Sion (2001) used *Hubble Space Telescope* (*HST*) spectra of the Lyα line to measure the temperature, surface gravity and spectroscopic orbit of the DAO white dwarf. They combined these data with observations from ground-based observatories to measure the masses and radii of the DAO and K-dwarf stars to an accuracy of about 7 per cent. They find that the DAO star has the radius expected for its mass but that the K-dwarf is 18 per cent larger than normal Hyades dwarfs of the same mass. They attribute this expansion to the large degree of coverage of the stellar surface by starspots. They find that the white dwarf in V471 Tau is the most massive one known in the Hyades but also the hottest and youngest, in direct conflict with expectation. They suggest that V471 Tau may be the result of the evolution of a triple-star system.

O'Donoghue et al. (2003) report the discovery of eclipses in the white dwarf–M-dwarf binary EC 13471−1258. They also used *HST* observations combined with observations from ground-based observatories to measure the masses and radii of the stars. They were able to achieve an accuracy of 5–10 per cent in these measurements despite the complications that arise from the extreme flaring behaviour of the M-dwarf. They find that the radius of the white dwarf is that expected for a carbon–oxygen white dwarf and that the M-dwarf also has the same radius as normal dwarf stars of the same mass. O'Donoghue et al. argue that the M-dwarf just fills its Roche lobe and that this, combined with the rapid rotation of the white dwarf, strongly suggests that the system has undergone mass transfer in the past, and imply that it is a hibernating cataclysmic variable (CV).

Maxted et al. (2004) report the discovery of eclipses in the white dwarf–M-dwarf binary RX J2130.6+4710. They present light curves and spectroscopy from which they derive masses to an accuracy of about 5 per cent and radii to an accuracy of about 10 per cent for both stars. There is no secondary eclipse visible in the light curves of this binary so Maxted et al. used the amplitude of the ellipsoidal effect as an additional constraint in their analysis to resolve the degeneracy between inclination and the ratio of radii of the stars. They find that the radius of the white dwarf is that expected for a carbon–oxygen white dwarf and that the M-dwarf also has the same radius as normal dwarf stars of the same mass.

There are several other white dwarf–M-dwarf binaries known, some of which are eclipsing binaries (Hillwig, Honeycutt & Robertson 2000). These tend to be systems in which the light from the secondary star is dominated by reprocessed radiation from the hot white dwarf. This light is asymmetrically distributed on the surface of the M-dwarf and often produces a spectrum dominated by emission lines, so some model of the 'reflection effect' is required to infer dynamical masses from the the spectroscopic orbit. It is usually the case for these binaries that there is insufficient information to determine the masses of the stars without assuming that one of the stars has a normal radius for its mass. Alternatively or additionaly, it may be necessary to use a surface gravity estimate for the white dwarf derived by fitting synthetic spectra to the observed spectrum to determine the geometry of the binary.

Schreiber & Gänsicke (2003) have made a compilation of measured and estimated masses, radii and effective temperatures for white dwarf–M-dwarf binaries and other post common-envelope binaries. They considered the past and future evolution of these binaries based on these parameters. They find that the sample of known post common-envelope binaries is very incomplete. In particular, the majority of post common-envelope binaries that will evolve into CVs within a Hubble time (pre-CVs) are missing from existing surveys because the white dwarf is too cool to stand out from it's companion star. Much of this analysis is based on indirect estimates of the masses and radii mentioned above. One reason to study binaries like RR Cae, RX J2130.6+4710, EC 13471−1258 and V471 Tau is to test the accuracy of the methods used to make these indirect estimates.

In this paper, we present new spectroscopy and photometry of RR Cae. We derive the spectroscopic orbit of the white dwarf and determine the mass ratio of the binary directly. We present photometry in white light of the eclipse from which we derive an accurate ephemeris. We combine an analysis of our white-light data and spectroscopic orbits with cooling models for the white dwarf to measure the mass and the radius of the M-dwarf in RR Cae. In contrast to previous studies, we find that the radius and mass of the M-dwarf are normal for a star of this spectral type.

2 OBSERVATIONS & REDUCTIONS

2.1 Photometry

We observed RR Cae with a photomultiplier photometer on the 0.75- and 1.0-m telescopes at the South African Astronomical Observatory (SAAO) near Sutherland, South Africa. These data were obtained unfiltered (i.e. in 'white-light') with 1-s continuous integrations. The blue sensitive photocathode of the detector thus provides a very broad response equivalent to the combination of Johnson $U + B + V$ passbands. The data were reduced by subtracting sky and correcting for extinction using an appropriate mean extinction coefficient.

We also observed RR Cae using the SAAO 0.75-m telescope using the UCT CCD photometer. The UCT CCD is a Wright Instruments Peltier-cooled camera with a 576 × 420 thinned, back-illuminated EEV charge-coupled device (CCD). The plate scale of the resulting images is 0.37 arcsec per pixel. Observations were obtained on 11 nights in the interval 1999 December 7–20. We first subtracted the bias value calculated from overscan regions from all the images. We used the median value of several images of the twilight sky devoid of bright stars to calculate a flat-field calibration image which was then normalized and applied to all the images of RR Cae. We used optimal photometry (Naylor 1998) to determine instrumental magnitudes of the stars in each frame. There are three comparison stars in the images we obtained, althought they are all 3–4 mag fainter than RR Cae in the I band. In total, we obtained over 3000 images of RR Cae. There are clear differences from night-to-night in the differential magnitudes we have calculated. This is due to a combination of several effects, including intrinsic variability of RR Cae, differential extinction between RR Cae and the comparison stars and inaccuracies in the flat-fielding. This latter effect is particularly acute for our UCT CCD images because the twilight sky is a different colour to the night sky and the stars themselves. This results in systematic errors that vary with the position of the stars

in the CCD images and the airmass. For these reasons, we have only used these data to measure the depth and times of primary eclipse.

2.2 Spectroscopy

Observations of RR Cae were obtained with the grating spectrograph on the SAAO 1.9-m Radcliffe Telescope. The detector was a SITe CCD with 1798 pixels 15 μm wide in the direction of dispersion. We used a 1200 line mm^{-1} grating and a 1.5-arcsec slit to obtain 66 spectra with a resolution of about 1 Å covering the wavelength region 4050–4915 Å at a dispersion of 0.5 Å $pixel^{-1}$. Observations were obtained on the nights 1999 December 15–19. We used the same instrument to obtain 15 spectra with a resolution of about 0.85 Å covering the wavelength region 8365–8975 Å at a dispersion of 0.35 Å $pixel^{-1}$ on the night 1999 December 20. The signal-to-noise ratio (S/N) in our spectra is typically 5–10.

Extraction of the narrow-slit spectra from the images was performed automatically using optimal extraction to maximize the S/N of the resulting spectra (Marsh 1989). The arcs associated with each stellar spectrum were extracted using the same weighting determined for the stellar image to avoid possible systematic errors due to the tilt of the spectra on the detector. The wavelength scale was determined from a fourth-order polynomial fit to measured arc line positions. The standard deviation of the fit to the arc lines was typically one-tenth of a pixel. The wavelength scale for an individual spectrum was determined by interpolation to the time of mid-exposure from the fits to arcs taken before and after the spectrum to account for the small amount of drift in the wavelength scale (<0.2 Å) due to flexure of the instrument between arc spectra. Statistical errors on every data point calculated from photon statistics are rigorously propagated through every stage of the data reduction.

3 ANALYSIS

3.1 Ephemeris

We have used our white-light photometry to establish an ephemeris for the times of primary minimum. We measured the time of mid-eclipse from the light curve around each eclipse observed using a least-squares fit of a very simple light-curve model. The model is based on the eclipse of one circular disc with uniform surface brightness by another circular disc. The measured times of minimum and their standard errors are given in Table 1. The precision of each measurement was calculated from the covariance matrix of the least-squares fit. Times are reported as Barycentric Julian date on the Barycentric Dynamical Time (TDB) time-scale, which we refer to as Barycentric Julian Dynamical date (BJDD). Corrections from UTC to BJDD were calculated using routines from SLALIB version 2.4–5 (Wallace 2000). The corrections vary from (UTC−TDB) = 61.7 to 64.4 s for these data.

We found that the χ^2 statistic for a least-squares fit of a linear ephemeris was much larger than expected for a good fit (χ^2 = 2357 *cf.* an expected value of 8). This problem is reduced but not removed by using a quadratic ephemeris (χ^2 = 125 *cf.* an expected value of 7). The poor fit is caused by variations of a few seconds in the observed time of minimum compared to the predicted time. We defer a discussion of the source of this variabilty to Section 4, but note here that this is a night-to-night variation, not a long-term trend. To allow for this additional source of noise in the eclipse timings we added an 'external error', $\sigma_{\rm ext}$, in quadrature to the standard error values given in Table 1. The value of $\sigma_{\rm ext} = 4.2$ s was chosen to give a reduced χ^2 value close to 1 for the least-squares fit to the data used to establish the following linear ephemeris:

$$\mathrm{BJDD(Mid-eclipse)} = (2\,451\,523.048\,567 \pm 0.000\,019) + (0.303\,703\,6366 \pm 0.000\,000\,0047)\mathrm{E}.$$

All phases quoted in this paper have been calculated with this ephemeris. The residuals from this ephemeris are shown in Fig. 1 and tabulated in Table 1.

We also used a least-squares fit to the same data to determine a quadratic ephemeris. We used a value of $\sigma_{\rm ext} = 3.8$ s to give a

Table 1. Times of mid-eclipse for RR Cae. The source of the data are indicated as follows: R – Bruch & Diaz (1998); W – white-light data from this paper, I – *I*-band data from this paper and K – Krzeminski (1984). The cycle number and residual from our linear ephemeris, O−C, are also given. Note that only the white-light data are used to determine the ephemeris.

BJDD(Mid-eclipse)	Cycle	O−C (s)	Source
2445927.91665	−18423	15.6	K
2449721.478524 ± 0.000003	−5932	−6.1	W
2449722.389675 ± 0.000003	−5929	−2.7	W
2449726.337828 ± 0.000004	−5916	−2.2	W
2450681.78958	−2770	7.5	R
2450684.82703	−2760	43.2	R
2450687.86361	−2750	3.8	R
2450688.77470	−2747	2.0	R
2450688.77477	−2747	8.0	R
2450700.619201 ± 0.000004	−2708	7.1	W
2450750.426547 ± 0.000002	−2544	2.7	W
2450753.463587 ± 0.000002	−2534	3.0	W
2450756.500622 ± 0.000002	−2524	2.9	W
2451045.626463 ± 0.000002	−1572	1.1	W
2451523.35226 ± 0.00003	1	−0.9	I
2451524.56706 ± 0.00005	5	−1.9	W
2451524.56707 ± 0.00003	5	−1.3	I
2451528.51518 ± 0.00004	18	−4.5	I
2451532.46335 ± 0.00003	31	−2.6	I
2453228.648145 ± 0.000002	5616	−3.9	W

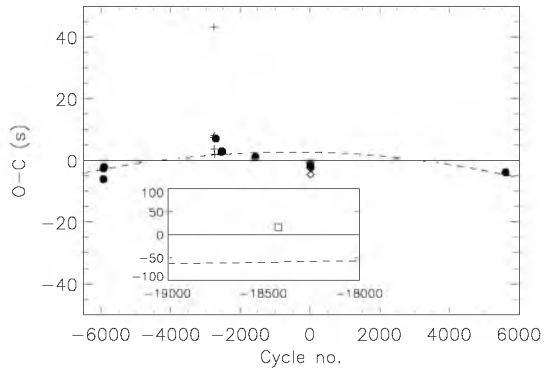

Figure 1. Residuals from a linear ephemeris for our measured times of mid-eclipse. Symbols are as follows: dots – white-light data from this paper; crosses – Bruch & Diaz (1998); open diamonds – *I*-band data from this paper and open square (inset, note change of scale) – Krzeminski (1984). Note that only the white-light data are used to determine the ephemeris. The difference between the times of minimum predicted by our quadratic and a linear ephemerides is shown using a dashed line.

reduced χ^2 value close to 1.

$$\mathrm{BJDD(Mid-eclipse)} = (2\,451\,523.048\,560 \pm 0.000\,018) + (0.303\,703\,6340 \pm 0.000\,000\,0035)\mathrm{E} - (2.27 \pm 0.79) \times 10^{-12}\mathrm{E}^2.$$

We are not confident that this is a significant detection of a period change in RR Cae because the level of significance depends on having reliable standard errors for the observed times of minimum, which is clearly not the case here, and the coefficient of E^2 is strongly dependent on the single observation on JD 2453228. However, we can confidently state that the period of RR Cae has not changed by more than $|\dot{P}|/P \approx 5 \times 10^{-12}$ over a time-scale of 10 yr.

Other observed times of minimum and their residuals from the linear ephemeris presented above are given in Table 1. We used our simple light-curve model to measure the time of mid-eclipse from our *I*-band photometry. We measured the full width at half minimum depth of the eclipse from our mean white-light light curve and found a value of 0.027254 ± 0.000001 in phase units. We used this value to convert the times of mid-ingress and mid-egress given by Bruch & Diaz (1998) to times of mid-eclipse. We have experimented with fitting all these data to determine an ephemeris but find that this makes a negligible change to the results presented above. One early time of minimum is given by Krzeminski (1984). The uncertainty in this value is not available so it is not clear whether it provides a useful constraint on $|\dot{P}|/P$.

3.2 The spectroscopic orbit of the white dwarf

The S/N in the individual spectra is rather low so we created 20 phase-binned spectra over the phase range 0.0 to 1.0, that is, the weighted average of the observed spectra in groups taken at the same orbital phase to within 0.05 phase units. Our blue spectra show three broad absorption lines from the white dwarf due to Hβ, Hγ and Hδ. Narrow emission lines from the M-dwarf are seen near the centre of these broad absorption lines. A few weak absorption features from the M-dwarf, particularly molecular bands, are present at the red end of the spectrum.

To measure the radial velocity of the white dwarf from the Balmer lines we used a two-stage least-squares fit of multiple Gaussian profiles to the spectra independently for each Balmer line. The spectra were normalized using a linear least-squares fit to a region of the spectrum either side of the Balmer line. To achieve a good fit to the absorption line we used the sum of two Gaussian profiles with the same velocity but independent widths and depths. A single Gaussian profile was deemed to be a poor fit to these broad absorption lines. We used a single Gaussian profile to model the Balmer emission line and included a first order polynomial in the fit to model the continuum. The first least-squares fit was used to establish the optimum widths and depths of the Gaussian profiles by fitting all the spectra simultaneously. The position of the absorption line was calculated from the radial velocity predicted by the expression $V_r = \gamma_{\mathrm{WD}} - K_{\mathrm{WD}} \sin(2\pi\phi)$, where ϕ is the phase. A similar expression using γ_{em} and K_{em} was used for the emission line. The values of γ_{WD}, K_{WD}, γ_{em} and K_{em} were included as free parameters in the fit. Only data within 1000 km s^{-1} of the rest wavelength of the line where included in the fit. The second least-squares fit we used to measure the radial velocity of the white dwarf in each spectrum independently. The widths and depths of the Gaussians used to model the white dwarf absorption were fixed at the values measured in the first step. The free parameters in the fit were the radial velocity of the white dwarf, the width and height of the emission line, the radial velocity of the emission line and the coefficients of the polynomial used to model the continuum. The width and height of the emission lines were optimized individually for each spectrum so that the radial velocity measurements of the white dwarf were not affected by poor fits to the emission lines. The fits to the spectra around the Hβ line are shown as a trailed grey-scale plot in Fig. 2. Examples of the second least-squares fit to the spectra at two key phases are shown in Fig. 3. We attempted to subtract an estimate of the M-dwarf spectrum from the observed spectra to improve the least-squares fit but found that this had a negligible effect on the results.

We used an unweighted least-squares fit to the measured radial velocites for the white dwarf to determine the optimum values of γ_{WD} and K_{WD} using the same expression for V_{r} as above. For the observed value of the radial velocity at each phase we used the

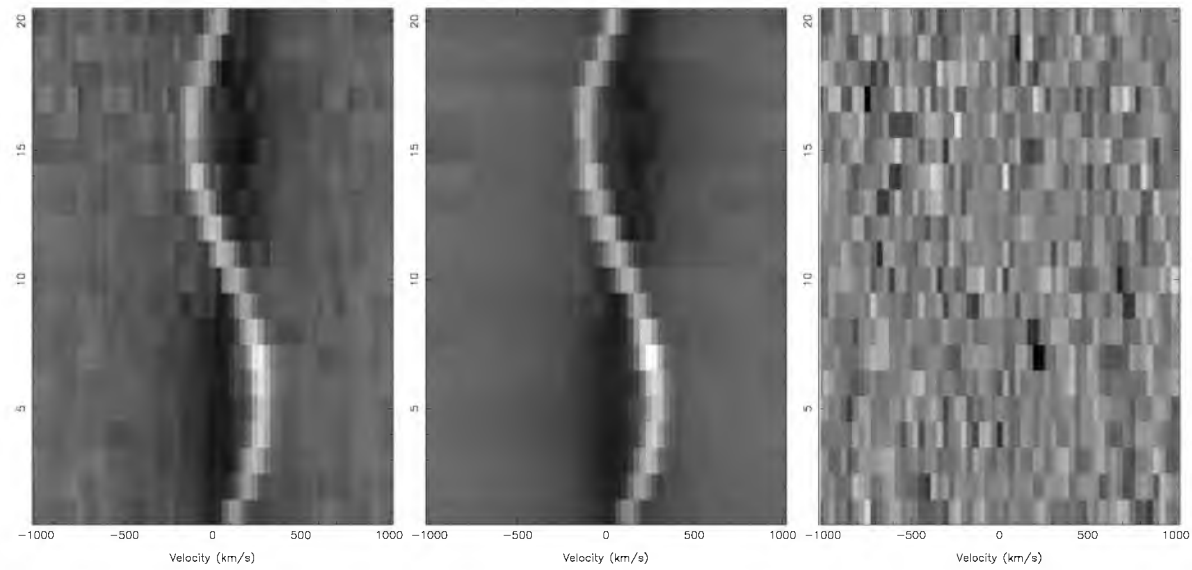

Figure 2. Trailed grey-scale spectra of the Hβ line in RR Cae. Left-to-right: observed, phase-binned spectra; least-squares fit; residuals from the fit. For the spectra, white is an intensity value of 1.25, black is 0.25. For the residuals, the intensity scale is −0.2 to +0.2 from white to black.

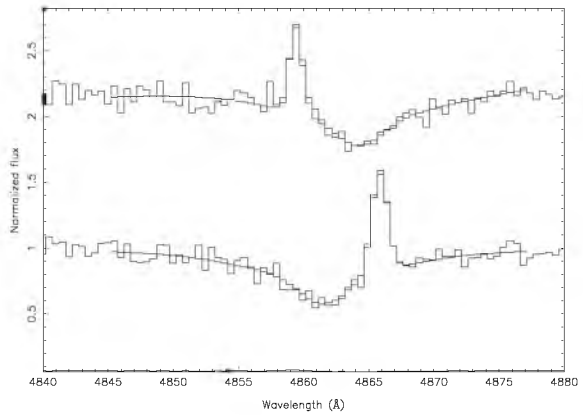

Figure 3. Examples of multiple Gaussian least-squares fits to the Hβ line. Two spectra of RR Cae are shown (thin line) together with the model spectra (thick line). The upper spectrum and fit have been offset vertically by 1.2 units for clarity.

Table 2. Circular orbit fits. All velocities are in units of km s^{-1}. N is the number of observations included in the least-squares fit. The two values of N and σ given in the column headed 'M-dwarf' refer to the radial velocity measurements of the absorption line spectrum presented here and from Bruch (1999), respectively. The least-squares fit accounts for the effect of the exposure time on the value of K derived.

	White dwarf	M-dwarf	Emission lines
γ	81.5 ± 2.1[a]	85.8 ± 3.6	80.1 ± 1.0
K	79.3 ± 3.0	190.2 ± 3.5	196.3 ± 1.4
σ	9.0	7.3, 11.9	4.6
N	20	14, 21	20

[a]See the text for a discussion of the reliability of this estimate.

weighted mean of the values from the three Balmer lines, excluding one unreliable measurement for the Hδ line. The resulting fits are given in Table 2. Also shown in Table 2 are the values of $\gamma_{\rm em}$ and $K_{\rm em}$ determined in the same way. The measured radial velocities and sinusoidal fits are shown in Fig. 4. It should be noted that it is difficult to establish an accurate continuum level for the spectra given the noise in the spectra, the contamination of white dwarf spectrum by the M-dwarf and the lack of any spectrophotometric standard star observations to calibrate the instrument response. This is likely to lead to a systematic error in the radial velocities measured from the broad white dwarf absorption lines. However, all the spectra will be affected in a similar way so we expect that this will only affect our estimate of $\gamma_{\rm WD}$. These systematic effects should have a negligible affect on our estimate of $K_{\rm WD}$.

3.3 The spectroscopic orbit of the M-dwarf

We measured the radial velocity of the M-dwarf in RR Cae from our spectra over the region 8440–8930 Å by cross-correlation. We chose these wavelength limits to avoid the parts of the spectrum with strong telluric absorption. We used a variety of spectra of M-dwarfs taken from the study of Cenarro et al. (2001) as templates for the cross correlation. We found that the choice of template has a negligible effect on the results. The results presented here used the spectrum of the M5-6 dwarf BD +19° 5116 B as a template spectrum. These data have a well defined zero-point but insufficient phase coverage to reliable determine the value of $K_{\rm M}$. Bruch (1999) provides similar radial velocity measurements for the M-dwarf which do have good

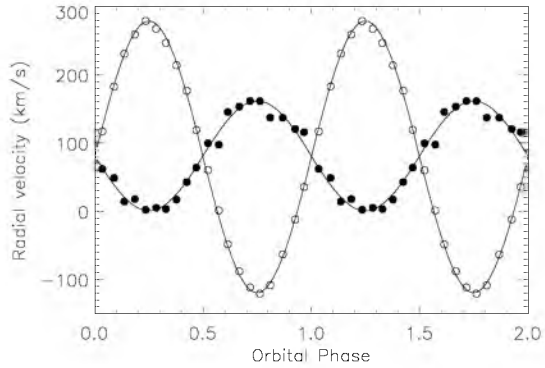

Figure 4. Measured radial velocities for the white dwarf (filled circles) and Balmer emission lines (open circles).

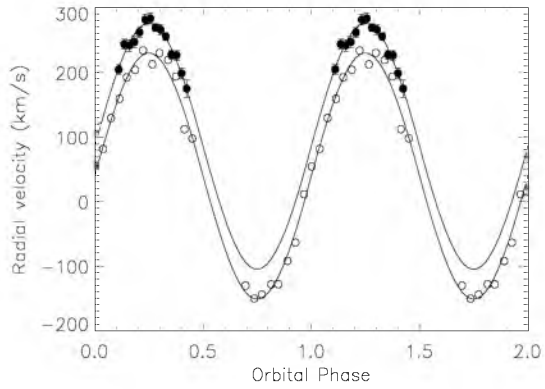

Figure 5. Measured radial velocities for the M-dwarf from Bruch (1999) (open circles) and from this paper (filled circles). Least-squares sinusoidal fits with independent means but the same semi-amplitude are also shown. Standard errors for radial velocities from this paper are shown as error bars. The standard error for the Bruch & Diaz measurements is assumed to be 12 km s^{-1}.

phase coverage but the zero-point for those measurements is not well defined. Therefore, we have used a weighted least-squares fit to our radial velocity measurements and the radial velocities tabulated by Bruch (1999) of two sinusoidal functions with independent means but a common semi-amplitude $K_{\rm M}$. The radial velocities were weighted according to their standard errors. The standard errors for our radial velocity measurements were calculated from the parabolic fit to the three highest points in the cross-correlation function plus an additional uncertainty of 2.6 km s^{-1} added in quadrature to achieve a reduced χ^2 value of 1 in the least-squares fit. We used the rms residual value from a least-squares fit of a sine wave to the Bruch radial velocities only to estimate a standard error of 12 km s^{-1} for those measurements. The results of the least-squares fit to both data sets are given in Table 2 and are shown in Fig. 5.

3.4 The light curve

The light curve of RR Cae shows that the white dwarf is totally eclipsed for 10 min 04 s and the ingress and egress phases last 1 min 50 s (Fig. 6). The depth of the eclipse varies from 2.6 mag in white-light to 0.25 mag in the I band.

For a given inclination, i, a single eclipse will give an accurate measurement of the radii of the stars relative to their separation, that is, $r_{\rm WD} = R_{\rm WD}/a$ and $r_{\rm M} = R_{\rm M}/a$, where a is the separation of the stars and $R_{\rm WD}$, $R_{\rm M}$ are the radii of the white dwarf and the M-dwarf,

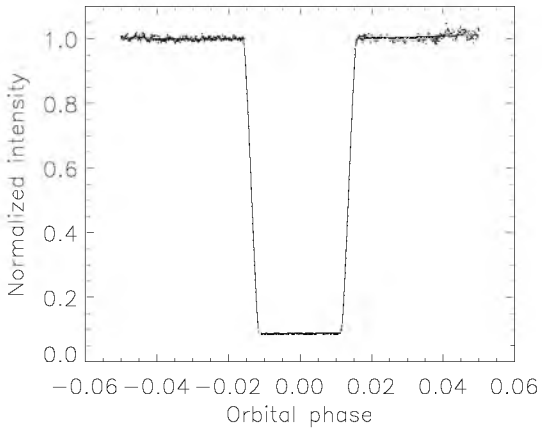

Figure 6. The mean white-light light curve of RR Cae (points) and a least-squares fit for a uniform disc eclipse (solid line, barely visible). The mean light curve is the average of all our white-light photometry in the phase range −0.05 to 0.05 resampled into 1001 bins.

respectively. Additionally, the depth of the eclipse gives an accurate measurement of the luminosity ratio, l_λ at the effective wavelength of the light curve, λ. Good fits to the eclipse can be found for a wide range of i values.

We used least-squares fits to our white-light photometry of the light-curve model EBOP (Etzel 1981; Popper & Etzel 1981) to measure the functions $r_{\rm WD}(i)$ and $r_{\rm M}(i)$ over a grid of inclination values from 76° to 90° in 2° steps. We fitted each eclipse we had observed separately and used the standard error of the mean for the results to estimate the standard error in $r_{\rm WD}(i)$ and $r_{\rm M}(i)$ at each value of i. The data from JD 2450700 were excluded from the analysis because they give discrepant results, for reasons that will be discussed below. The value of $r_{\rm WD}$ depends slightly on the limb darkening values adopted for the white dwarf. Atmospheres of DA white dwarfs usually consist of pure hydrogen. However, in the case of RR Cae the presence of a number of metal lines indicates significant contamination by heavy elements, which alters the structure of the atmosphere and thus the limb-darkening coefficient. A detailed determination of the abundance mix is beyond the scope of this paper. For this reason we consider a wide range of linear limb darkening coefficients from $u_1 = 0.35$ to 0.95 in steps of 0.2. The values of $r_{\rm WD}(i)$ and $r_{\rm M}(i)$ we derive are shown in Fig. 7. It is clear that the standard errors contribute negligibly to the uncertainty in $r_{\rm WD}(i)$ and $r_{\rm M}(i)$ and that the value of $r_{\rm M}(i)$ does not depend on u_1. We also show the mean of the rms values for the least-squares fits to the light curves to demonstrate that there is very little difference in the goodness of fit for a wide range of inclination.

3.5 The effective temperature of the white dwarf

Bragaglia, Renzini & Bergeron (1995) estimated the white dwarf parameters from model atmosphere fits to the Balmer lines. However, that analysis is seriously hampered by the uncorrected contamination of the spectrum by the light of the M-dwarf companion. Here, we present an analysis which overcomes this shortcoming.

RR Cae was observed as part of the Supernovae Type Ia Progenitor Survey (SPY – Napiwotzki et al. 2001). Spectra were taken with the high-resolution echelle spectrograph UVES attached to the UT2 telescope of VLT. The SPY setup used for the UVES observations provides almost complete spectral coverage from 3200 to 6650 Å

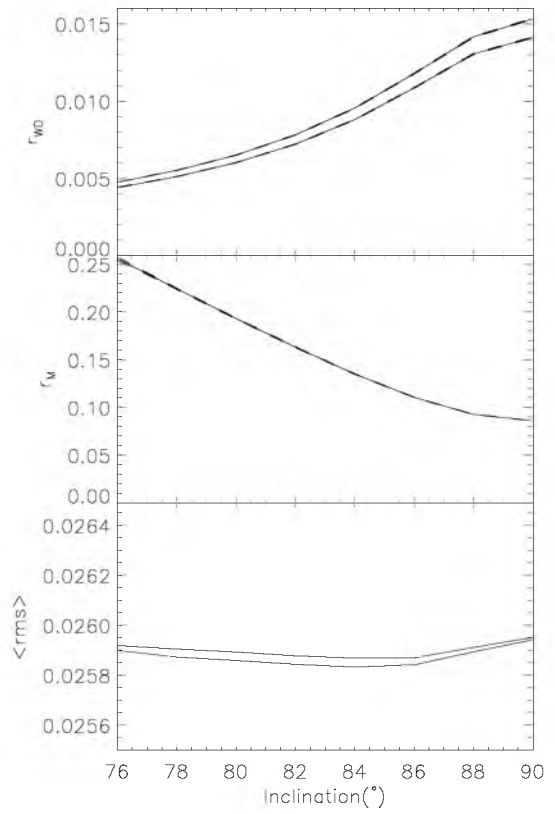

Figure 7. Upper panel: the optimum value of $r_{\rm WD}$ as a function of inclination from a least-squares fit to our white-light photometry using a linear limb darkening coefficient of $u_1 = 0.35$ (lower solid line) or 0.95 (upper solid line). The standard error in each curve is indicated using a dashed line either side of optimum value (barely visible). Middle panel: the optimum value of $r_{\rm M}$ as a function of inclination from a least-squares fit to our white-light photometry (solid line). The standard error in the curve is indicated using a dashed line either side of optimum value (barely visible). The effect of the limb-darkening coefficient of the white dwarf is negligible. Lower panel: the mean rms for the least-squares fits the normalized data for individual eclipses. Results are shown for an assumed linear limb darkening coefficient of $u_1 = 0.35$ (lower curve) and $u_1 = 0.95$ (upper curve).

with a resolution of about 0.3 Å. Further details of the observations and data reduction are given in Napiwotzki et al. (2001).

The analysis was performed with the FITSB2 code, which is designed to perform a model atmosphere analysis of double lined binary systems in which both components are visible (Napiwotzki et al. 2004). Radial velocities and stellar parameters of both components can be treated as free parameters. The spectrum of the white dwarf in RR Cae was modelled with a grid of spectra computed with the model atmosphere code of Detlev Koester described in Finley, Koester & Basri (1997). The spectrum of the M-dwarf was modelled using template spectra from the library of stellar spectra of Cincunegui & Mauas (2004). This library contains flux-calibrated high-resolution spectra. Spectral type is used as the fit parameter for the M-dwarf.

Relative flux contributions at 6700 Å from the white dwarf and the M-dwarf were fixed at the value $F_{\rm WD}/F_{\rm Mstar} = 1.68$ derived by Bruch & Diaz (1998) from their light-curve analysis. As a first step, we made use of the full spectral range from the Balmer lines to Hα to constrain the spectral type and radial velocities of the M-dwarf. White dwarf parameters were allowed to vary as well during this phase. We estimate the spectral type of the M-dwarf to

be about M4. For the final fit to the spectrum we restricted the fit to the Balmer lines Hβ and higher with M-dwarf parameters fixed at the previously measured values. We used two spectra taken at epochs HJD=2 451 889.7315 and 2 451 891.6927 for this analysis. The final fit is compared to one of the observed spectra in Fig. 9.

The resulting white dwarf parameters are $T_{\rm eff} = 7540\,{\rm K}\pm175\,{\rm K}$ and $\log g = 7.97$. The standard error in $T_{\rm eff}$ is taken to be 2.3 per cent (Napiwotzki, Green & Saffer 1999). The uncertainty in the value of $\log g$ is discussed in Section 4. The new temperature is higher than the Bragaglia et al. (1995) value, indicating a somewhat smaller cooling age than assumed previously.

3.6 Masses and radii of the stars

For each value of i and u_1 we can combine the value of $r_{\rm WD}$ and $r_{\rm M}$ with the spectroscopic orbits in Table 2 to derive the masses and radii for the stars. To estimate a nominal value of u_1 we refer to the linear limb darkening coefficients calculated by Claret (2000)) for the Johnson U, B and V filters for $T_{\rm eff} = 6750$, 7000, and 7250 K, $\log g = 4.5$, 5.0 and $\log[M/H] = -4.5$ (where $[M/H]$ is the heavy metal abundance relative to the Sun). Extrapolating to the $\log g$ value of RR Cae, we estimate that the value of u_1 likely to be about 0.65 ± 0.15. We have adopted a large standard error on this estimate to reflect the uncertainty due to extrapolating over a large range of $\log g$ and the poorly defined band-pass for our white-light photometry. Fortunately, the actual value of u_1 adopted has a negligible effect on our results.

The masses and radii we derive for the stars as a function of inclination are shown in Fig. 8. Also shown in Fig. 8 are the mass–radius relations for white dwarfs with various compositions from the cooling models of Benvenuto & Althaus (1999). As we have no further useful observational constraint on the inclination we use the range of radii for the white dwarf predicted by these models to find the likely range of radii for the M-dwarf. The range of values we derive for the radii of the stars are given in Table 3 and are shown as thick, solid lines in Fig. 8. We see that the masses of the stars are well determined and the main source of uncertainty in the white dwarf radius is the unknown mass of the surface hydrogen layer. We use the value of $K_{\rm M}$ measured from the absorption line spectrum of the M-dwarf to estimate the masses because the emission lines may arise from regions that are not uniformly distributed over the surface of the M-dwarf. Although the value of $K_{\rm em}$ is more precise than $K_{\rm M}$ it may not accurately reflect the orbital motion of the centre-of-mass of the M-dwarf.

We have used a Monte Carlo technique to estimate the uncertainties on the masses and radii we have measured. For each of 1000 trials we select random deviates from a normal distribution for every quantity that is used to calculate the masses and radii, that is, $K_{\rm WD}$, $K_{\rm M}$, u_1, $r_{\rm WD}(i)$ and $r_{\rm M}(i)$. We use two values of i corresponding to the extreme values of $R_{\rm WD}$ found for cooling models with thin and thick hydrogen layers. We then calculate and store the masses and radii of the stars for every trial so that we can calculate their standard deviations and the correlation between the parameters. The standard errors derived are given in Table 3. The joint confidence region for the mass and radius of the M-dwarf are shown as an ellipse in the lower panel of Fig. 8.

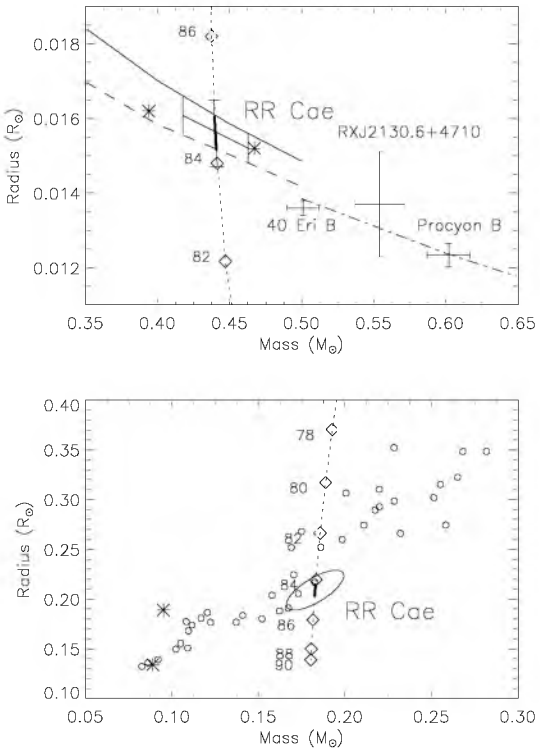

Figure 8. Upper panel: the mass–radius relation for RR Cae and other white dwarfs. The predicted mass–radius relation from the cooling models of Benvenuto & Althaus (1999) is shown as follows: dashed line – helium white dwarf with a thin hydrogen layer ($X = 10^{-8}$), $T_{\rm eff} = 7540$ K; solid line – helium white dwarf with a thick hydrogen layer ($X = 4 \times 10^{-4}$), $T_{\rm eff} = 7540$ K; dash–dotted line – CO white dwarf with thin hydrogen layer ($X = 10^{-8}$), $T_{\rm eff} = 10\,000$ K. The dotted line show the relation between mass and radius for RR Cae inferred from our light curves and the spectroscopic orbit. Diamonds on this line are labelled by the corresponding inclination in degrees. The thick, solid line shows the intersection of this relation with the models. The thin capped solid line extending from this thick line show the 68.3 per cent confidence interval for the radius. The thin, almost-horizontal, solid lines forming the error bar show the 68.3 per cent confidence interval for the mass at the best estimate of the white dwarf mass and radius. The mass and radius of the white dwarf RX J2130.6+4710 from Maxted et al. (2004) is shown. Also shown are the masses and radii of Procyon B and 40 Eri B from Provencal et al. (2002). The estimates for the mass and radius from Bruch (1999) and Bruch & Diaz (1998) are shown as asterisks. Lower panel: The M-dwarf component of RR Cae in the mass–radius plane compared to other M-dwarfs taken from Clemens et al. (1998). The thick, solid line and the dotted line are the mass and radius corresponding to the white dwarf mass and radius in the panel above. The ellipse is the 68.3 per cent confidence region for the M-dwarf mass and radius for the best estimate of the masses radius. The estimates for the mass and radius from Bruch (1999) and Bruch & Diaz (1998) are shown as asterisks.

4 DISCUSSION

The mass we have derived for the M-dwarf in RR Cae is very different from the much lower masses given by Bruch (1999) or Bruch & Diaz (1998). Our analysis is more reliable than those studies because we have measured a dynamical mass ratio for the stars from the spectroscopic orbits. In contrast to those studies, we find that the radius of the M-dwarf is consistent with its mass (Fig. 8) and our estimate of the spectral type (Leggett 1992). We fully agree with the statement of Bruch (1999) that the uncertainty ranges quoted in that study 'do not take into account the correlation between parameters. Thus, they must not be mistaken as errors of the corresponding parameters!'.

In principle, the gravitational redshift of the white dwarf can be used as an additional constraint to determine a unique solution for

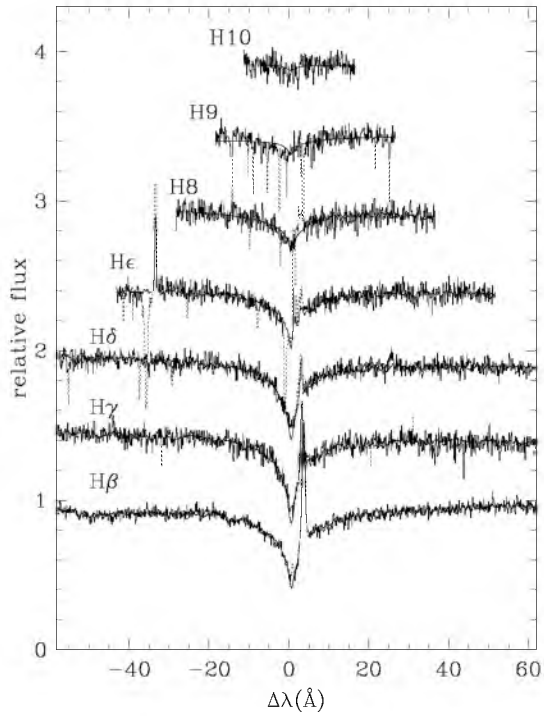

Figure 9. Determination of the white dwarf parameters by a model atmosphere fit of the composite spectrum of RR Cae (spectrum taken at HJD 2 451 889.7315 shown here). The M-dwarf spectrum is computed for parameters determined in a previous step (see text). Dotted lines indicate M star emission lines and photospheric white dwarf metal absorption lines excluded from the fit.

Table 3. The masses (M), radii(R), effective temperatures ($T_{\rm eff}$) and surface gravities (g) of the stars in RR Cae. Where a range of values are given this reflects the range of values calculated from different cooling models for the white dwarf. The uncertainty quoted is a standard deviation for a fixed mass and radius derived from a Monte Carlo analysis. N.B. the errors in the masses and radii are correlated (see Fig. 8).

Parameter	White dwarf	M-dwarf
$M(\mathrm{M}_\odot)$	0.440 ± 0.023	$(0.182–0.183) \pm 0.012$
$R(\mathrm{R}_\odot)$	$(0.015–0.016) \pm 0.0004$	$(0.203–0.215) \pm 0.015$
$T_{\rm eff}$ (K)	7540 ± 175	3100 ± 100^a
$\log g$(cgs)	$(7.67–7.72) \pm 0.06$	$(5.04–5.09) \pm 0.04$

[a]Based on our estimate of the spectral type and the calibration of Leggett (1992).

the masses and radii of the stars independently of the white dwarf cooling models. The gravitational redshift of the white dwarf is expected to be about 17 km s^{-1}. This is clearly not consistent with the values of $\gamma_{\rm WD}$ and $\gamma_{\rm M}$ we have measured. We believe this is due to a systematic error in our value of $\gamma_{\rm WD}$ (see Section 3.2). The UVES spectra discussed in Section 3.5 yield two radial velocities per star which we estimate have uncertainties of a few km s^{-1}. Since the phase of the observations is known this is sufficient to estimate the values of $\gamma_{\rm WD}$, $\gamma_{\rm M}$, $K_{\rm WD}$ and $K_{\rm M}$. We find that the values of $K_{\rm M}$ and $K_{\rm WD}$ are consistent with the values shown in Table 2 to within a few km s^{-1}. The difference $\gamma_{\rm WD} - \gamma_{\rm M} \approx 10$ km s^{-1} is closer to the expected value than the value in Table 2.

The surface gravity of the white dwarf, $\log g$, derived from the analysis of the spectrum is larger than the range computed from the orbital solution and light-curve analysis given in Table 3 by about 0.3 dex. Systematic errors of this type in the value of $\log g$ for cool white dwarfs have been noted by several authors (Bergeron et al. 1990; Bergeron, Wesemael & Fontaine 1992; Kleinman et al. 2004) but the reasons for this effect are not clear. It has been suggested that the effect is a result of an increase in the mean mass of the samples towards cooler temperatures. This clearly cannot apply in the case of RR Cae. The mass implied by the values of $T_{\rm eff}$ and $\log g$ derived in Section 3.5 is about 0.57 $\mathrm{M}_\odot$ for a cooling model with a hydrogen layer thickness of 10^{-4} (Benvenuto & Althaus 1999).

We have calculated the time-scale for circularization by tidal forces of the orbit in RR Cae and find that it is only a few thousand years. For this reason, we discount the suggestion by Bruch (1999) that there is a significant eccentricity in the orbit. We do not speculate here on the origin of the feature in the R-band light-curve offset from phase 0.5 which he suggests may be a secondary eclipse, but note that our radius measurements for the stars in RR Cae predict that the secondary eclipse has a depth of 7 mmag or less.

We have recalculated the past and future evolution of RR Cae using the analysis described by Schreiber & Gänsicke (2003) but with our new, more accurate values for the masses and radii of the stars. The cooling age, $t_{\rm cool}$, of RR Cae derived by interpolating the cooling tracks of Wood (1995) is $\log (t_{\rm cool}/y) = 8.94$. This is the time since RR Cae emerged from the common-envelope phase, at which time the orbital period is estimated to have been 0.31–0.32 d depending on the prescription used to model the angular momentum loss due to a magnetic stellar wind in this interval. The continued loss of angular momentum will shrink the Roche lobe of the M-dwarf to the point where mass transfer will start from the M-dwarf to the white dwarf through the inner Lagrangian point. RR Cae will then be a cataclysmic variable star (CV). This will occur at an orbital period $P_{\rm sd} = 0.080$–0.086 d. Our estimate of the time before Roche lobe overflow occurs, $t_{\rm sd}$, also depends on the prescription for angular momentum loss used and varies from $\log (t_{\rm sd}/y) = 9.94$ to $\log (t_{\rm sd}/y) = 10.3$. These values are not much changed from those presented by Schreiber & Gänsicke (2003), but the changes are sufficient to alter two of their conclusions. First, the revised value of $P_{\rm sd}$ is at the lower limit of the range 2–3 h in which very few non-magnetic CVs are observed (the CV period gap) rather than within this period range. Secondly, the value of $t_{\rm sd}$ for RR Cae may be consistent with the definition of a pre-CV used by Schreiber & Gänsicke (2003), that is, post-common envelope binaries that evolve into a semidetached configuration in less than the Hubble-time.

We have also used the prescriptions for angular momentum loss described in Schreiber & Gänsicke (2003) to calculate the current rate of period change, $\dot{P}/P$, for RR Cae. We find that for classical magnetic braking, (Verbunt & Zwaan 1981) $\dot{P}/P \approx 5 \times 10^{-14}$ and for revised magnetic braking, (Pinsonneault, Andronov & Sills 2002) $\dot{P}/P \approx 1.4 \times 10^{-13}$. In either case, we would not expect to detect any period change given the accuracy of our eclipse timings. Continued monitoring of the eclipse times of RR Cae will, in principle, enable us to distinguish between these two prescriptions for magnetic braking, although the predicted change in period is only sufficient to change the predicted time of minimum by about 1 s over 10 yr.

A concerted observing campaign will be required to reliably measure such a small change in the orbital period of RR Cae, particularly in the presence of the additional source of noise identified from our white-light photometry. We have considered several possibilities for the source of this additional error. There is no evidence for systematic errors in the photometry at phases outside eclipse large enough to account for the changes in eclipse timings were similar systematic

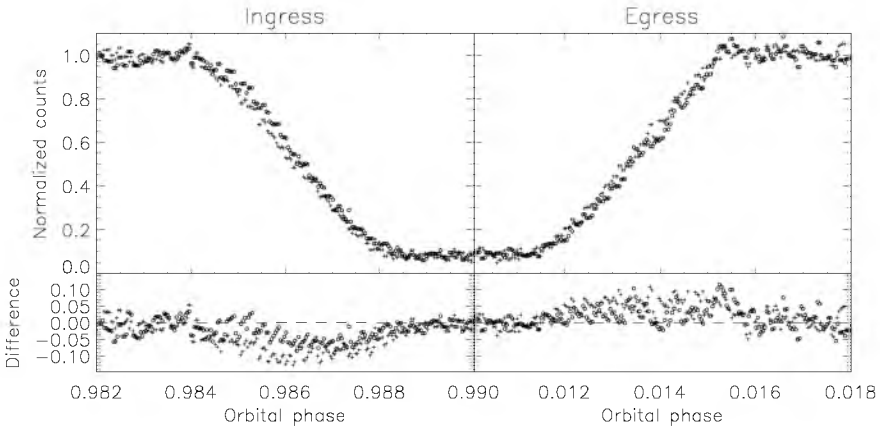

Figure 10. A comparison of two eclipses observed on consecutive nights with the SAAO 1-m telescope using white-light photoelectric photometry. The data are from the nights 1995 January 03 (crosses) and 1995 January 04 (open circles). The light curves have been normalized independently to a mean out-of-eclipse level of 1 and smoothed using a three-point median filter. The difference between these light curves and the average light curve shown in Fig. 6 is also shown below each portion of the light curve.

errors to occur during the eclipse. Careful inspection of the residuals shows that the ingress and egress phases are not affected equally, so the external noise source is not errors in the timing of the observations. We looked for the influence of flares from the M-dwarf on the eclipse timings but did not see any flare-like features in the light curves of any significance.

Watson & Dhillon (2004) describe how the Wilson effect can perturb the eclipse timings of eclipsing binaries like RR Cae by a few seconds. Their simulation of the Wilson effect shows that the cause of the change in eclipse timing is a shift of the whole ingress or egress phase of the eclipse. In Fig. 10, we compare two eclipses taken on subsequent nights, both of which are a few seconds early compared to our linear ephemeris but by clearly different amounts (2.7 and 6.1 s). We see that the reason for this difference is a change of shape of the ingress phase, not a simple shift. This is particularly notable in the difference between these light curves and the mean light curve in the phase range 0.985–0.986. There is also an overall shift to the time of ingress and egress compared to the mean light curve. We conclude that the Wilson effect may contribute to the variability in the times of mid-eclipse but some other phenomenon is also contributing to these variations.

We also considered the possibility that the white dwarf in RR Cae has star spots due to a magnetic field similar to those seen in the cool white dwarf WD 1953−011 (Maxted et al. 2000; Brinkworth et al. 2005). The detection of sharp metal lines in the spectrum of RR Cae by Zuckerman et al. (2003) would appear to rule out this possibility because we would expect these lines to show strong Zeeman splitting in this scenario. In order to produce the variability we observe in RR Cae the viewing angle between the observer and the hypothetical spot must change. At some orientations the line of sight will be along the magnetic field lines, in which case the longitudinal field produces a split pair of circularly polarized σ components in the spectral line and suppresses the central linearly polarized π component (Rutten 1996), that is, the orientation of the magnetic field is favourable for the detection of Zeeman splitting. Strong Zeeman splitting of the lines will not be apparent if the orbital and spin axes of the white dwarf are aligned with the magnetic field, but this orientation does not give rise to any rotational modulation of the brightness.

Rather than a dark spot due to a strong magnetic field, it may be that bright regions on the white dwarf due to accretion may contribute to the variability of the eclipse timings. Accretion from the solar-like wind of the M-dwarf is thought to be responsible for the presence of sharp metal lines in the spectrum of RR Cae (Zuckerman et al. 2003). This hypothesis can be tested by looking for correlations between the overall apparent brightness of the white dwarf and the presence of distortions to the eclipse light curve. If the distortions to the light curve seen in Fig. 10 are interpreted as changes in brightness of the white dwarf then the overall brightness changes at blue wavelengths are expected to be quite large (about 5 per cent). The mass transfer rate on to the white dwarf required to generate an accretion luminosity equal to 5 per cent of the white dwarf luminosity is $3 \times 10^{-14}\,\mathrm{M}_{\odot}\,\mathrm{yr}^{-1}$. Debes (2006) has calculated the accretion rate on to the white dwarf implied by the observed abundance of Ca II in the atmosphere of RR Cae and the corresponding mass-loss rate from the M-dwarf assuming Bondi–Hoyle accretion. They find a mass accretion rate $\dot{M} = 4 \times 10^{-16}\,\mathrm{M}_{\odot}\,\mathrm{yr}^{-1}$ and a mass loss rate $\dot{M}_{\mathrm{RD}} = 6 \times 10^{-16}\,\mathrm{M}_{\odot}\,\mathrm{yr}^{-1}$. This can be compared to the upper limit to the mass-loss rate of $\leqslant 2 \times 10^{-15}\,\mathrm{M}_{\odot}\,\mathrm{yr}^{-1}$ for the M5.5 dwarf Proxima Cen (Wood et al. 2001). If accretion on to the white dwarf is responsible for the distortions to the light curve then the M-dwarf in RR Cae is much more active than Proxima Cen and/or the mass transfer on to the white dwarf is very non-uniform. Intriguingly, a footnote to a table in Zuckerman et al. for RR Cae notes 'accretion disc/hotspot on WD?', though it is not clear what leads the authors to make this suggestion.

The DAB white dwarf HS 0209+0832 appears to be an example of a WD with no significant magnetic field that shows variations of chemical abundances over the surface (Heber et al. 1997). RR Cae is much cooler than HS 0209+0832 so the hydrogen is almost completely neutral. In these conditions trace metals are an important sources of free electrons and opacity. Variations in chemistry across the surface of RR Cae similar to those seen in HS 0209+0832 may result in local changes in the atmospheric structure that may be related to the variability in eclipse shape that we have seen. In summary, none of the explanations above is entirely satisfactory but some progress may be made by looking for variability in the strength of the metal lines in RR Cae.

Bruch (1999) found that the equivalent width of the Hα emission lines is variable by about 50 per cent with a tendency for the line be brighter at phases close to eclipse. This is exactly the opposite of the behaviour expected if the emission line is due to irradiation of the M-dwarf by the white dwarf. Our measurements of the equivalent

width of the Balmer emission lines are not as accurate as those of Bruch because the lines are weaker in the higher Balmer lines. Some variability is apparent, but this is not coherent with orbital phase, for example, a flare-like brightening of the Hβ line is apparent around phase 0.3 in Fig. 2. This enforces the conclusion of Bruch that the emission lines are the result of chromospheric activity on the M-dwarf.

ACKNOWLEDGMENTS

Based on observations obtained at the South African Astronomical Observatory. PFLM and LMR were supported by a PPARC post-doctoral grants. The calculation of the eclipsed area for our simple light-curve model is taken from a BASIC code written by Dan Bruton of the Department of Physics & Astronomy, Stephen F. Austin State University, Texas. We thank Detlev Koester for providing us with a grid of model atmospheres. We thank the referee for comments on the manuscript that have helped us to clarify several points in the text.

REFERENCES

Benvenuto O. G., Althaus L. G., 1999, MNRAS, 303, 30
Bergeron P., Wesemael F., Fontaine G., Liebert J., 1990, ApJ, 351, L21
Bergeron P., Wesemael F., Fontaine G., 1992, ApJ, 387, 288
Bragaglia A., Renzini A., Bergeron P., 1995, ApJ, 443, 735
Brinkworth C. S., Marsh T. R., Morales-Rueda L., Maxted P. F. L., Burleigh M. R., Good S. A., 2005, MNRAS, 357, 333
Bruch A., 1999, AJ, 117, 3031
Bruch A., Diaz M. P., 1998, AJ, 116, 908
Cenarro A. J., Cardiel N., Gorgas J., Peletier R. F., Vazdekis A., Prada F., 2001, MNRAS, 326, 959
Claret A., 2000, A&A, 363, 1081
Clemens J. C., Reid I. N., Gizis J. E., O'Brien M. S., 1998, ApJ, 496, 352
Cincunegui C., Mauas P. J. D., 2004, A&A, 414, 699
Debes J. H., 2006, ApJ, 652, 636
Etzel P. B., 1981, in Carling E. B., Kopal Z., eds, Photometric and Spectroscopic Binary Systems. NATO ASI Ser. C., 69, Dordrecht, p. 111
Finley D. S., Koester D., Basri G., 1997, ApJ, 488, 375
Heber U., Napiwotzki R., Lemke M., Edelmann H., 1997, A&A, 324, L53
Hillwig T. C., Honeycutt R. K., Robertson J. W., 2000, AJ, 120, 1113
Kleinman S. J. et al., 2004, ApJ, 607, 426
Krzeminski W., 1984, IAU Circ. 4014
Leggett S. K., 1992, ApJS, 82, 351
Marsh T. R., 1989, PASP 101, 1032
Maxted P. F. L., Ferrario L., Marsh T. R., Wickramasinghe D. T., 2000, MNRAS, 315, L41
Maxted P. F. L., Marsh T. R., Morales-Rueda L., Barstow M. A., Dobbie P. D., Schreiber M. R., Dhillon V. S., Brinkworth C. S., 2004, MNRAS, 355, 1143
Napiwotzki R., Green P. J., Saffer R. A., 1999, ApJ, 517, 399
Napiwotzki R. et al., 2001, AN, 322, 411
Napiwotzki R. et al., 2004, ASPC, 318, 402
Naylor T., 1998, MNRAS, 296, 339
O'Brien M. S., Bond H. E., Sion E. M., 2001, ApJ, 563, 971
O'Donoghue D., Koen C., Kilkenny D., Stobie R. S., Koester D., Bessell M. S., Hambly N., MacGillivray H., 2003, MNRAS, 345, 506
Pinsonneault M. H., Andronov N., Sills A., 2002, ASPC, 261, 208
Popper D. M., Etzel P. B., 1981, AJ, 86, 102
Provencal J. L., Shipman H. L., Koester D., Wesemael F., Bergeron P., 2002, ApJ, 568, 324
Rutten R. L., 1996, Radiative Transfer in Stellar Atmospheres, Lecture Notes, 3rd edn. Utrecht University, p. 32.
Schreiber M. R., Gänsicke B. T., 2003, A&A, 406, 305
Verbunt F., Zwaan C., 1981, A&A, 100, L7
Wallace P. T., 2000, SLALIB Programmer's Manual, Starlink User Note, 67.61, CCLRC/Rutherford Appleton Laboratory
Watson C. A., Dhillon V. S., 2004, MNRAS, 351, 110
Wood M. A., 1995, LNP, 443, 41
Wood B. E., Linsky J. L., Müller H.-R., Zank G. P., 2001, ApJ, 547, L49
Zuckerman B., Koester D., Reid I. N., Hünsch M., 2003, ApJ, 596, 477

This paper has been typeset from a TEX/LATEX file prepared by the author.